AGU100 ADVANCING EARTH AND SPACE SCIENCE

Geophysical Research Letters

RESEARCH LETTER
10.1029/2018GL079263

Key Points:
- Spatial heat heterogeneities are imaged on a frictional interface using carbon properties and Raman spectroscopy
- Rupture processes become more efficient with increasing slip on fault
- Heating efficiency depends on time-dependent *memory effect* of the fault surface

Supporting Information:
- Supporting Information S1

Correspondence to:
J. Aubry,
jerome.aubry@ens.fr

Citation:
Aubry, J., Passelègue, F. X., Deldicque, D., Girault, F., Marty, S., Lahfid, A., et al. (2018). Frictional heating processes and energy budget during laboratory earthquakes. *Geophysical Research Letters*, *45*, 12,274–12,282. https://doi.org/10.1029/2018GL079263

Received 20 JUN 2018
Accepted 1 NOV 2018
Accepted article online 5 NOV 2018
Published online 28 NOV 2018

Frictional Heating Processes and Energy Budget During Laboratory Earthquakes

J. Aubry[1], F. X. Passelègue[2], D. Deldicque[1], F. Girault[3], S. Marty[1], A. Lahfid[4], H. S. Bhat[1], J. Escartin[3], and A. Schubnel[1]

[1]Laboratoire de Géologie, École Normale Supérieure/CNRS UMR 8538, PSL Research University, Paris, France, [2]École Polytechnique Fédérale de Lausanne, Lausanne, Switzerland, [3]Institut de Physique du Globe de Paris, Sorbonne Paris Cité, Université Paris Diderot, CNRS UMR, Paris, France, [4]Bureau de Recherches Géologiques et Minières, Orléans, France

Abstract During an earthquake, part of the released elastic strain energy is dissipated within the slip zone by frictional and fracturing processes, the rest being radiated away via elastic waves. While frictional heating plays a key role in the energy budget of earthquakes, it could not be resolved by seismological data up to now. Here we investigate the dynamics of laboratory earthquakes by measuring frictional heat dissipated during the propagation of shear instabilities at stress conditions typical of seismogenic depths. We estimate the complete energy budget of earthquake rupture and demonstrate that the radiation efficiency increases with thermal-frictional weakening. Using carbon properties and Raman spectroscopy, we map spatial heat heterogeneities on the fault surface. We show that an increase in fault strength corresponds to a transition from a weak fault with multiple strong asperities and little overall radiation, to a highly radiative fault behaving as a single strong asperity.

Plain Language Summary In nature, earthquakes occur when the stress accumulated in a medium is released by frictional sliding on faults. The stress released is dissipated into fracture and heat energy or radiated through seismic waves. The seismic efficiency of an earthquake is a measure of the fraction of the energy that is radiated away into the host medium. Because faults are at inaccessible depths, we reproduce earthquakes in the laboratory under natural in situ conditions to understand the physical processes leading to dynamic rupture. We estimate the first complete energy budget of an earthquake and show that increasing heat dissipation on the fault increases the radiation efficiency. We develop a novel method to illuminate areas of the fault that get excessively heated up. We finally introduce the concept of spontaneously developing *heat asperities*, playing a major role in the radiation of seismic waves during an earthquake.

1. Introduction

During an earthquake, the elastic strain energy accumulated during the interseismic period is released by rapid fault sliding. The resulting ground shaking depends in large part on the dynamics (Das, 2007) and the energy budget of rupture propagation (Kanamori & Brodsky, 2004; Kanamori & Rivera, 2006): $E_{tot} = E_R + G_c + Q_{th}$, where E_{tot} is the total potential (elastic strain) energy and E_R is the energy radiated away by elastic waves. Fracture energy G_c is the energy required to weaken the fault, allowing the fracture to propagate further and includes all the energy spent to create a new fault surface (Griffith, 1920) and form gouge and microcracks at the crack tip or near the rupture front (Ide, 2002). Q_{th} is the energy dissipated locally by frictional heating (Kanamori & Rivera, 2006). In the last decade, several studies have proposed that frictional heating activates thermal mechanical processes explaining the dynamic evolution of fault strength, such as grain size reduction and superplastic flow (Green et al., 2015; Verberne et al., 2013), thermal pressurization of pore fluid (Rice, 2006; Wibberley & Shimamoto, 2005), flash heating (Goldsby & Tullis, 2011; Rice, 2006), frictional melting (Di Toro et al., 2006; Hirose & Shimamoto, 2005), and mineral phase transformations (Brantut et al., 2011; Schubnel et al., 2013). All of these mechanisms result in significant fault weakening during seismic slip (Di Toro et al., 2011), through a process that is largely controlled by temperature evolution on the fault plane, hence raising concern that the theoretical partitioning between fracture energy and frictional heat is ill-posed because both energy terms contribute actively to fault weakening.

On the other hand, seismological observations have shown a high variability of rupture speed (Chounet et al., 2017; Ide, 2002; Kanamori & Brodsky, 2004), stress drop (Allmann & Shearer, 2009; Brune, 1970), and radiation

efficiency (Ide et al., 2007; Kanamori & Brodsky, 2004), which solely depends on the radiated and fracture energies (Kanamori & Brodsky, 2004). However, while the radiated energy is well-estimated using accelerograms (Boatwright, 1980), fracture energy, inferred from scaling laws and stress drops, has large uncertainties (Abercrombie & Rice, 2005; Tinti et al., 2005; Wong, 1982) and frictional heat remains *invisible* to seismological data. As a consequence, field studies along active or fossil fault zones (Chester et al., 2005; Di Toro et al., 2006; Ma et al., 2006; Ohnaka, 2003; Savage et al., 2014), numerical modeling (Bhat et al., 2007; Madariaga, 1976; Madariaga et al., 1998; Noda et al., 2013), and laboratory experiments (Lockner et al., 2017; Nielsen et al., 2016; Passelègue et al., 2016) have been carried out to further constrain the energy budget of earthquakes. Among these approaches, reproducing earthquakes in the laboratory under controlled thermodynamic conditions, as analogs of natural earthquakes (Brace & Byerlee, 1966), may well provide a unique opportunity to understand the physics of the earthquake source.

In this paper, we investigate the seismic energy budget during stick-slip events on Westerly granite under confining pressures typical of the brittle crust. We used two complementary approaches to constrain the energy balance of laboratory earthquakes. Temperature is measured near the fault surface to quantify frictional heat produced during sliding. For the first time, spatial heat heterogeneities on the fault plane are imaged at the small scale after frictional sliding.

2. Materials and Methods

2.1. Sample Characterization and Preparation

The rock material is Westerly granite, a reference for rock mechanics experiments under crustal conditions (Scholz, 1986). It is composed of 33% of potassic feldspars, 33% of plagioclase, 28% of quartz, 5% of phyllosilicates (biotite and muscovite), and 1% of accessory minerals (Scholz, 1986). In the experiments, we used cylindrical samples 80 mm in length and 40 mm in diameter that were sawed to create an interface at 30° with respect to the vertical axis (Figure 1a). First, the two surfaces of the saw-cut fault plane were polished with a surface grinder and then roughened with #240 grit sandpaper. Second, a rectangular carbon layer (10 mm × 20 mm) with a maximum thickness of 30 nm was deposited on the center of the top surface using a carbon coater that allowed a uniform evaporation. Then, a thermocouple was inserted in the footwall sample 5.5 mm away from the contact surface. Finally, the sample was isolated from the confining oil by a neoprene jacket (125-mm long, 5-mm wall thickness).

2.2. Experimental Setup

The triaxial oil-loading cell used for the experiments is an autocompensated triaxial cell installed at the Laboratoire de Géologie of École Normale Supérieure (Paris, France), which can reach 300 MPa confining pressure (Schubnel et al., 2005). Load point velocity applied during the experiments is 3 μm/s. Displacement is measured by a linear variable differential transducer, placed between the reaction frame and the top of the piston and corrected for machine stiffness. Parameters recorded during the experiment include displacement (±0.1 μm), axial (σ_1), and confining (σ_3) stresses (±0.01 MPa) and temperature (±0.01 °C) at a sampling rate of 100 Hz.

2.3. Mapping of Spatial Heat Heterogeneities With the Carbon Deposition Technique

To image frictional heating, we measured carbon spectra at the end of experiment, in the 850–2,000 cm^{-1} range, with the help of a Raman Micro-Spectrometer (Renishaw Invia, UK; argon laser beam of 514.5 nm; LEICA objective with 50× magnification) located at Bureau de Recherches Géologiques et Minières (Orléans, France). Spectra are composed of two principal bands named graphite (G band) and defect bands (D band) around 1,600 and 1,350 cm^{-1}, respectively. An increase in temperature induces an increase in the height of the D band on the Raman spectra compared with the initial spectra measured before experiment. The variation of the ratio of heights of D band to G band, H_d/H_g, allows identification of carbonization stages. The higher the degree of carbonization achieved, the higher the ratio (Deldicque et al., 2016). Before the experiment, the H_d/H_g ratio for carbon spectra is equal to 0.45 throughout the carbon layer. Post-mortem Raman Micro-Spectrometry mapping of carbon deposit on the top-wall fault plane (dimensions of 2 mm × 0.5 mm) provides carbonization maps for each experiment. Each pixel (10 × 10 μm^2) on the Raman Micro-Spectrometry map corresponds to one measured H_d/H_g ratio, which ranges between 0.45 and 1. When carbon spectrum was not measurable at a given location on the fault surface during

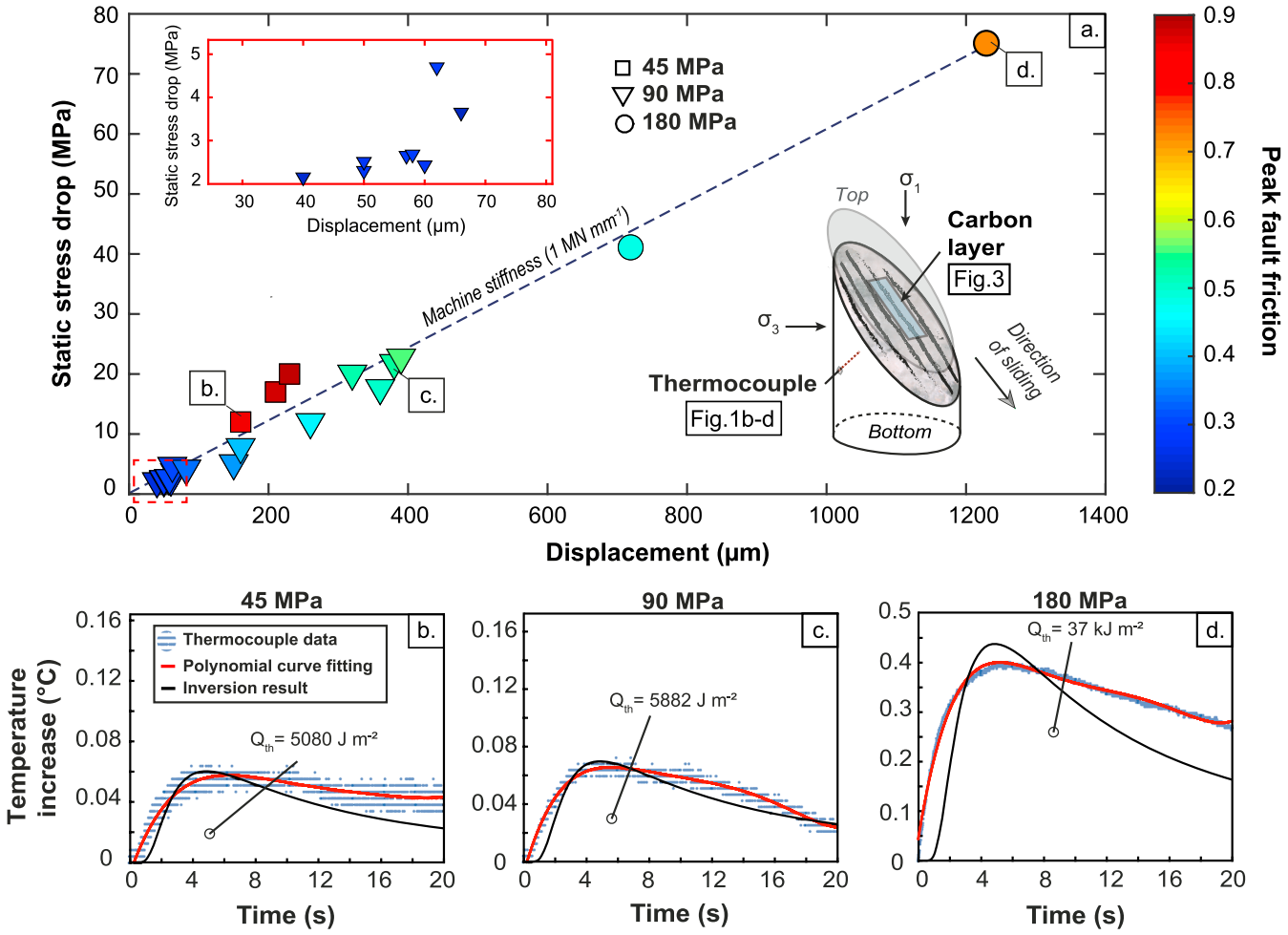

Figure 1. Mechanical and thermocouple data of laboratory earthquakes. (a) Static stress drop as a function of displacement and peak fault friction for the three confining pressures tested during triaxial experiments (45, 90, and 180 MPa). The inset at the top left-hand side is an enlargement of the small displacements region of the plot. The inset on the bottom right-hand side shows a schematic of the sample. The slope of the linear regression of the data points gives the machine stiffness of the triaxial loading cell. Temperature increase as a function of time for a single stick-slip event, shown in subplot (a), at confining pressures of 45, 90, and 180 MPa. We inverted the thermocouple data to calculate the frictional heat produced on the fault (section 2; Table S1). The amount of heat generated increases with the confining pressure. Raw thermocouple data are shown in blue, polynomial curve fitting in red, and the result of the inversion in black. Details on the thermal model are given in the supporting information.

mapping, we interpolated with the H_d/H_g ratios measured on neighboring pixels. H_d/H_g ratios allow us to quantify heat dissipation at the small scale on the interface, but there are important approximations in their conversion into temperatures (supporting information).

2.4. Temperature Measured by the Thermocouple

When a stick-slip occurs, the thermocouple (K-type, OMEGA, Norwalk, USA), installed at 5.5 mm away from the fault surface, records the evolution of the temperature at 100 Hz. Temperature data was then used to estimate the energy dissipated into heat during a given stick–slip event solving the one-dimensional heat equation in space and time with a finite difference scheme. Inverting a constant heat source throughout the duration of slip, t_w = 20 μs (measured as the characteristic time of weakening in Passelègue et al., 2016), the model outputs the best values of the frictional heat produced Q_{th} (J/m^2) to fit the experimental data 5.5 mm away from the fault surface (supporting information). Least-squares error minimization between the model and the experimental data was performed, considering a diffusion duration of 20 s. Parameters used for the inversions are: ρ the density of Westerly granite (2,650 kg/m^3); C the specific heat capacity of the rock (900 J·kg^{-1}·K^{-1}); t_w the duration of the event fixed at 20 μs (Passelègue et al., 2016); h the width

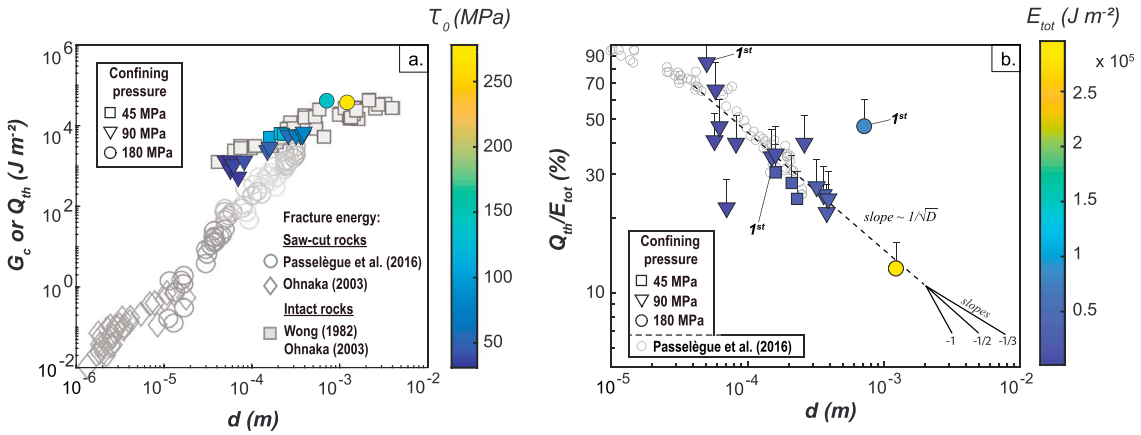

Figure 2. Frictional heat produced, fracture energy, and heating efficiency of laboratory earthquakes. (a) Frictional heat or fracture energy produced during stick-slip as a function of coseismic slip and peak shear stress. Experimental values of fracture energy versus slip from the literature are also plotted for saw-cut rocks (Ohnaka, 2003; Passelègue et al., 2016) and intact rocks (Ohnaka, 2003; Wong, 1982). The total heat produced during stick-slip, Q_{th}, increases with increasing coseismic slip, d. (b) Heating efficiency as a function of coseismic slip and total mechanical work. Black bars indicate the maximum contribution of latent heat (Table S1), calculated as $0.3 \times Q_{th}$ (supporting information). The occurrence of melting may not change the trend of the decrease of heating efficiency with slip. "1st" indicates the first stick-slip of a series of events, for each experiment. The theoretically expected evolution of heat generation appears to be consistent with our experimental observations.

of the sheared layer (m), defined as $h = 2(\pi\kappa t_w)^{1/2}$, where κ is the thermal diffusivity of Westerly granite (1×10^{-6} m^2/s). Additional information on the thermal model are given in the supporting information.

3. Results

3.1. Total Heat Produced During Laboratory Earthquakes

Three series of stick-slip experiments (Figure 1a) were conducted on saw-cut samples of Westerly granite at confining pressures of 45, 90, and 180 MPa. For each stick-slip, we measured the static stress drop, the coseismic displacement (corrected for elasticity), and the temperature evolution 5.5 mm away from the fault surface (Figure S1 in the supporting information). Within a series of stick-slip events, peak fault friction, static stress drops, and coseismic displacements increase with time. Static stress drops range from 2 MPa to 75 MPa, resulting in coseismic displacements ranging from 40 μm to 1.2 mm. As expected (Nielsen et al., 2016), the stress drop increases linearly with displacement and the relation follows the apparatus stiffness (Figure 1a). Stick-slip events with large stress drop and displacement are followed by clear temperature rises ranging from 0.04 °C to 0.4 °C (Figures 1b–1d).

Temperature measurements are inverted using a simple heat diffusion model (i.e., with one heat source point at 5.5 mm away from the fault surface) to quantify the heat produced coseismically by frictional sliding (Figures 1b–1d and Figure S2). The inversion fits the temperature evolution for experiments conducted at confining pressures of 45 and 90 MPa relatively well (Figures 1b and 1c). At confining pressure of 180 MPa (Figure 1d), the model cannot reproduce the data, which may be due to a thermal anomaly longer than the assumed 20 μs and to latent heat effects not considered in this study (supporting information).

The total heat produced during stick-slip increases with increasing coseismic slip and reaches up to 37 kJ/m^2 for the largest stick-slip event (Figure 2a). The comparison with previous measurements of fracture energy performed with the same setup under similar stress conditions (Passelègue et al., 2016) reveals that frictional heat dissipation is larger than fracture energy, particularly under low normal and shear stresses. This is expected because, under low normal and shear stress conditions, the frictional drop is low, resulting in small stress drop and low fracture energy. However, under higher normal and shear stress conditions, fracture energy and heat become comparable, which is consistent with the low dynamic friction and almost complete stress drops observed for larger slips (Di Toro et al., 2011; Passelègue et al., 2016). In summary, we confirm here, with two independent measurements of heat and fracture energy, that the large fracture energies measured during stick–slip events at high stress and large slips are dissipated by frictional heat rather than surface creation. Under these high stress conditions, most of the weakening is driven by thermal processes rather than fractures (Di Toro et al., 2011) and fracture energy can be neglected.

3.2. Surface Melting and Heating Efficiency

The evolution of fault strength during the initial stage of slip plays a crucial role in the fault-weakening processes (Hayward et al., 2016). Indeed, flash melting occurs at the onset of sliding (Beeler et al., 2008; Nielsen et al., 2008; Rice, 2006) for a small amount of slip (Renard et al., 2012), and at highly stressed frictional asperities during rapid slip (Rice, 2006). Postmortem Scanning Electron Microscope micrographs indeed reveal the presence of melt on the fault surfaces (Figures S3 and S4). At 45 MPa, most biotites and only a few plagioclases and potassic feldspars have melted. By contrast, all minerals including biotite, plagioclase, potassic feldspars, and even quartz fragments (minimum melting temperature of 1650 °C) have melted during experiments at 90 and 180 MPa, indicating that the temperature rise on the fault surface was larger during these experiments (Figures S3 and S4), thus facilitating an efficient melt lubrication of the fault (Di Toro et al., 2006).

The heating efficiency of our laboratory earthquakes shows a clear relation with the coseismic displacement. As stresses and displacements were measured continuously, the total (elastic strain) energy, $E_{tot} = (\tau_0 + \tau_r)d/2$, where τ_0 and τ_r are the initial and final shear stress (Pa), respectively, and d is the coseismic displacement (m), was also calculated for each stick-slip event. The heating efficiency, R, defined by the ratio of frictional heat produced Q_{th} to total work E_{tot}, decreases with increasing slip (Figure 2b). As the lubrication increases with confining pressure, this decrease of R is compatible with a low dynamic friction coefficient during large laboratory earthquakes (Table S1). Conversely, we argue that the true radiation efficiency in our experiments, that is, E_R/E_{tot}, must increase with increasing slip (i.e., increasing normal stress) to values close to 0.9. This is indeed supported by the fact that fracture energy is either negligible compared with heat at low normal stress and/or for small slip, or dissipated by frictional heat at larger stress and/or for larger slip. Our observations are also consistent with other laboratory experiments reporting close to complete stress drops (Brantut et al., 2016; Passelègue et al., 2016) and high (supershear) rupture speeds (Passelègue et al., 2013).

The apparent scaling of the heating efficiency R with the inverse of the square root of slip d ($R \propto d^{-1/2}$; Figure 2b) has strong implications for seismic efficiency. The heat produced per unit surface scales as $Q_{th} \propto \rho C \Delta T (\pi \kappa t_w)^{1/2}$, where ρ is the bulk density (kg/m^3), C the specific heat capacity (J·kg^{-1}·K^{-1}), ΔT the temperature rise on the fault plane (K), κ the thermal diffusivity (m^2/s) and t_w the duration of sliding (s), $(\pi \kappa t_w)^{1/2}$ being the thermal diffusion length (m). E_{tot} scales with the coseismic displacement, so that R scales as $d^{-1/2}$ only when Q_{th} scales as $d^{1/2}$. Our results show that, at our experimental scale, for similar apparent stress and stress drop, the heating efficiency decreases, and conversely the true radiation efficiency increases, with $d^{-1/2}$. Our experiments thus suggest that rupture processes become more efficient as sliding increases.

Heating efficiency is higher for the first stick-slips of a series and decreases with cumulative stick-slips events (Figure 2b), suggesting that less heat is generated by frictional sliding after cumulative displacements. We studied the effects of the number of stick-slips on the fault surface at confining pressure of 90 MPa (Figure S5). After a single stick-slip, we document the presence of gouge particles originating from minerals plucked along the fault interface. Agglomerated micro-particles and nanoparticles of gouge form strong asperities (exceeding hundreds of microns in length), which did not melt. After several stick-slips, molten gouge particles are found in microscale asperities (Figures S3–S5). These flattened melt patch asperities can be reworked by flash melting, which decreases the heating efficiency. Finally, the degree of shear deformation of the gouge and the amount of melt on the fault surface increase together with increasing confining pressure and slip (Figure S3). The effect of cumulative stick-slips shows that a given rupture event is controlled by the state of the fault surface, itself affected by the last rupture event through flash heating or frictional melting of minerals and the reworking of asperities (Figures 3 and S5). This suggests a time-dependent *memory effect* of the fault surface. The slip-dependent aggradation of asperities over their lifespan could be critical in natural crustal faulting as it may lead to more efficient seismic ruptures.

3.3. Imaging the Fault Surface Temperature During Slip

To image the spatial heat heterogeneities after frictional sliding, we used a method based on the carbon properties and the calculation of the H_d/H_g ratio (section 2). The H_d/H_g ratio is a measure of the maximized degree of carbonization reached on the fault surface during an entire seismic cycle. The use of this in situ carbon method provides several new insights on weakening processes of faulting. First, the average increase in the degree of carbonization achieved on the fault surface with increasing confining pressure (Figure 3) relates with the degree of shear melting imaged with Scanning Electron Microscope (Figure S3).

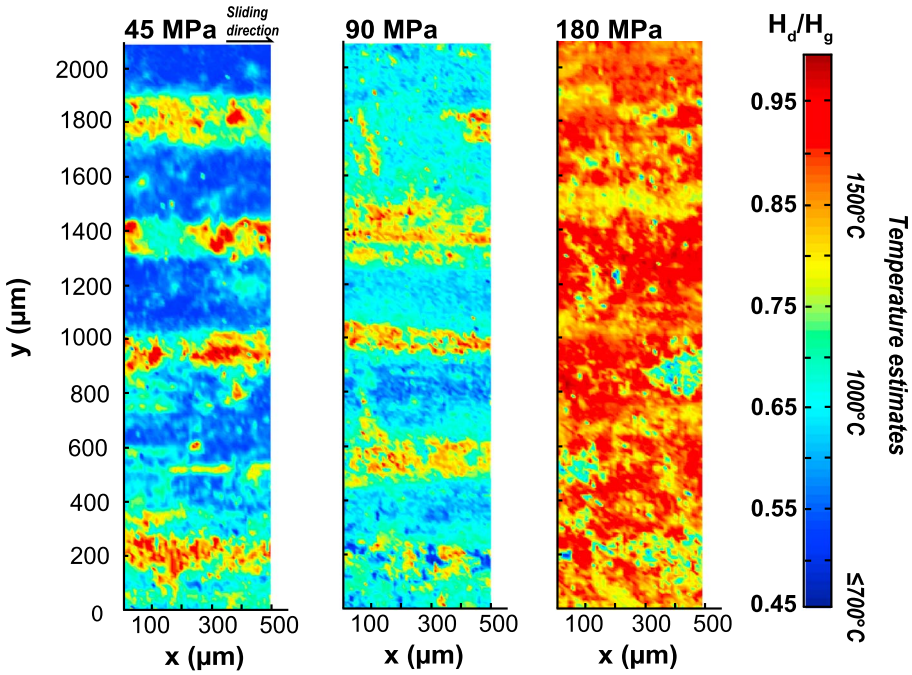

Figure 3. Carbonization maps during frictional sliding for three different confining pressures. Confining pressures of 45, 90, and 180 MPa are tested. The H_d/Hg ratio (i.e., degree of carbonization) reached on the fault increases with the confining pressure. During a laboratory earthquake, and over a few microns of slip, the fault surface reaches a heterogeneous and broad range of frictional heat production. Approximate temperatures can be converted from the H_d/H_g ratio. Sliding direction is parallel to the *x* axis. The temperature calibration method is detailed in the supporting information.

Second, for experiments conducted at confining pressures of 45 and 90 MPa, heat patches are laterally spread along the slip direction, approximately 100-µm wide and can be several hundreds of microns long (Figure 3). This geometry suggests a genetic link to asperities and striations on the fault plane. Indeed, *carbonized asperities* are longer than the maximum amount of coseismic displacement of any single stick-slip event during these two experiments. They therefore have remained active during several stick-slip events. At 180 MPa, asperities can no longer be recognized, but striations along the sliding direction remain visible.

Using a calibration (Figure S6), in which the cumulative effect of stick-slips, the heating duration, and the effects of shearing and shear strain on the carbonization of amorphous carbon were neglected due to equipment limitations (supporting information), we can infer approximate temperatures directly from the H_d/H_g ratio between 700 °C and 1800 °C. Although our calibration is only considered as a first step toward the estimation of precise temperature reached during stick-slips, it gives precious information on the thermal evolution of the fault surface at a never-before achieved spatial scale. These temperature estimates are consistent with temperatures for natural solidified frictional melts (i.e., pseudotachylytes) around 1100 °C in subduction context (Ito et al., 2017; Ujiie et al., 2007).

4. Discussion

Our series of experiments have important implications for natural earthquakes. We have shown that when the fault contact area is maximized and the fault plane entirely moltens, heating efficiency decreases with increasing coseismic slip and cumulative displacement. With increasing confining pressure and normal stress, we have observed the gradual transition from flash melting at asperity contacts to bulk melting over the fault surface. This important transition also corresponds to the transition from a weak fault, displaying few contact points, low driving shear stress, low stress drop, and high heating efficiency, to a strong fault having high contact area, high driving shear stress, high stress drop, and high radiation efficiency (Figure 4).

Seismological studies generally infer seismic radiation efficiency, $\eta = E_R/(E_R + G_c)$, ranging from zero for slow earthquakes (Ide et al., 2007) to one for large earthquakes (Venkataraman & Kanamori, 2004). Most

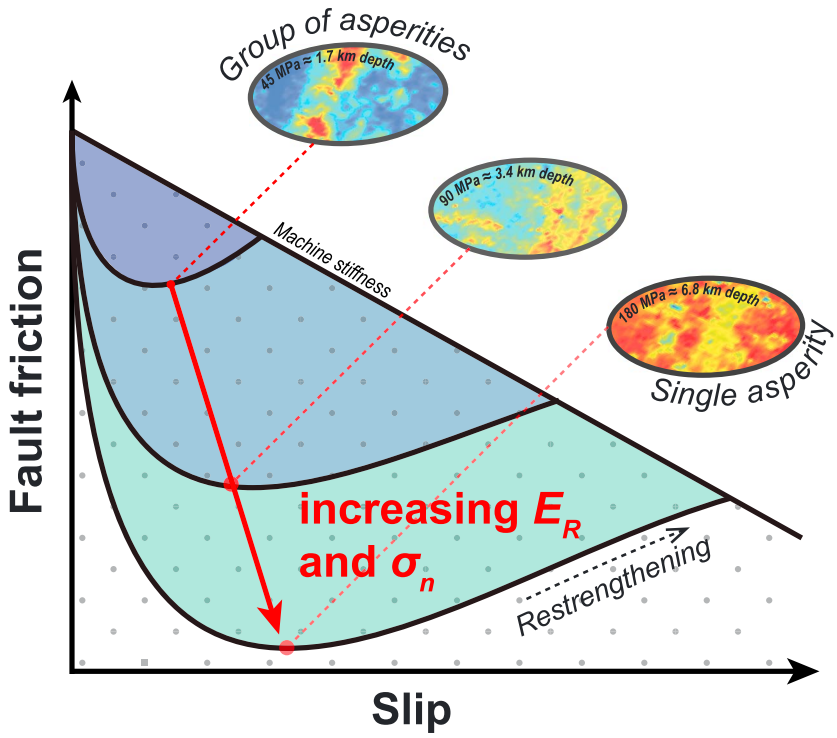

Figure 4. Schematic of friction evolution by combining thermocouple temperature measurements, heat distribution from carbon method, and energy budget. With increasing confining pressure, the mechanical behavior evolves from that of a group of asperities to that of a single asperity. When the fault surface is entirely molten, heat generation by frictional processes and fracture energy become low and radiated energy increases. Colored regions correspond to the radiated energy, E_R.

earthquakes, particularly along subduction zones, typically exhibit values of η between 0.3 and 0.8 (Lay et al., 2012; Venkataraman & Kanamori, 2004). Our observations suggest that moderate radiation efficiencies arise from rupture propagating along fault planes, where only a small portion of the rupture area is stressed (Figure 4). This stressed rupture area corresponds to asperities, which contribute greatly to the overall radiation efficiency of rupture, while the vast majority of the fault plane, which is relatively less stressed, shows limited stress drop and radiates poorly. Few earthquakes have been associated with radiation efficiency above one (Venkataraman & Kanamori, 2004), among them the 1992 Landers and 1994 Northridge earthquakes. Slip inversion studies (Wald et al., 1996; Wald & Heaton, 1994) have suggested that these earthquakes were dominated by the behavior of a single asperity whose size is comparable to the fault plane. Here we argue, on the basis of our experimental data, that these cases correspond instead to earthquakes with an apparent static stress drop much smaller than the dynamic stress drop on the asperity (Passelègue et al., 2016; Figure 4), as quenched frictional melt may weld the fault and lead to fast fault restrengthening and strength recovery (Ferrand et al., 2018; Mitchell et al., 2016).

5. Conclusion

In this paper, the dynamics of laboratory earthquakes has been investigated by measuring frictional heat dissipated during the propagation of shear instabilities. We have mapped spatial heat heterogeneities produced locally on the fault surface during coseismic slip. In addition, we have shown how the transition from the dynamics of a group of microscale asperities to that of a single asperity influences radiation efficiency, suggesting that radiation efficiency increases with thermal-frictional weakening. Our study therefore demonstrates that seismological radiation efficiencies larger than one are possible without the need to invoke frictional heating as a dominant energy sink. Under in situ pressure and temperature conditions, the difference between the complete radiative budget of earthquake rupture including heat and the seismological energy balance neglecting heat becomes negligible as radiation efficiency increases, at least at the scale of

asperities in the laboratory. Seismic radiation, thus, could be a larger component of the earthquake energy budget than is generally assumed.

Acknowledgments
We thank S. Bernard (IMPMC, Paris, France) and H. Lyon-Caen (ENS, Paris, France) for fruitful discussions. This study was funded by the European Research Council grant REALISM (2016-grant 681346) led by A. Schubnel. The authors declare that they have no competing financial interests. The manuscript has been greatly improved thanks to the constructive and thorough comments of two anonymous reviewers. Data presented in this study are listed in Table S1 in the supporting information. A. S., H. B., F. G., F. X. P., and J. E conceived the study. J. A, S. M., and A. S. performed the experiments. J. A., F. X. P., H. B., and A. S. performed the temperature inversion and energy budget discussion. J. A., A. L., and D. D. performed the Raman carbon temperature calibration and microstructural analyses. All authors participated equally to the redaction of the manuscript.

References

Abercrombie, R. E., & Rice, J. R. (2005). Can observations of earthquake scaling constrain slip weakening? *Geophysical Journal International*, *162*(2), 406–424. https://doi.org/10.1111/j.1365-246X.2005.02579.x

Allmann, B. P., & Shearer, P. M. (2009). Global variations of stress drop for moderate to large earthquakes. *Journal of Geophysical Research*, *114*, B01310. https://doi.org/10.1029/2008JB005821

Bangton, Z., Junqi, W., Hongfei, L., & Peirong, C. (2008). Estimating influence of crystallizing latent heat on cooling-crystallizing process of a granitic melt and its geological implications. *Acta Geologica Sinica-English Edition*, *82*(2), 438–443. https://doi.org/10.1111/j.1755-6724.2008.tb00594.x

Beeler, N. M., Tullis, T. E., & Goldsby, D. L. (2008). Constitutive relationships and physical basis of fault strength due to flash heating. *Journal of Geophysical Research*, *113*, B01401. https://doi.org/10.1029/2007JB004988

Bhat, H. S., Dmowska, R., King, G. C., Klinger, Y., & Rice, J. R. (2007). Off-fault damage patterns due to supershear ruptures with application to the 2001 *Mw* 8.1 Kokoxili (Kunlun) Tibet earthquake. *Journal of Geophysical Research*, *112*, B06301. https://doi.org/10.1029/2006JB004425

Boatwright, J. (1980). A spectral theory for circular seismic sources; simple estimates of source dimension, dynamic stress drop, and radiated seismic energy. *Bulletin of the Seismological Society of America*, *70*(1), 1–27.

Brace, W. F., & Byerlee, J. D. (1966). Stick-slip as a mechanism for earthquakes. *Science*, *153*(3739), 990–992. https://doi.org/10.1126/science.153.3739.990

Brantut, N., Han, R., Shimamoto, T., Findling, N., & Schubnel, A. (2011). Fast slip with inhibited temperature rise due to mineral dehydration: Evidence from experiments on gypsum. *Geology*, *39*(1), 59–62. https://doi.org/10.1130/G31424.1

Brantut, N., Passelègue, F. X., Deldicque, D., Rouzaud, J. N., & Schubnel, A. (2016). Dynamic weakening and amorphization in serpentinite during laboratory earthquakes. *Geology*, *44*(8), 607–610. https://doi.org/10.1130/G37932.1

Brune, J. N. (1970). Tectonic stress and the spectra of seismic shear waves from earthquakes. *Journal of Geophysical Research*, *75*(26), 4997–5009. https://doi.org/10.1029/JB075i026p04997

Chester, J. S., Chester, F. M., & Kronenberg, A. K. (2005). Fracture surface energy of the punchbowl fault, San Andreas system. *Nature*, *437*(7055), 133–136. https://doi.org/10.1038/nature03942

Chounet, A., Vallée, M., Causse, M., & Courboulex, F. (2017). Global catalog of earthquake rupture velocities shows anticorrelation between stress drop and rupture velocity. *Tectonophysics*, *733*, 148–158. https://doi.org/10.1016/j.tecto.2017.11.005

Das, S. (2007). The need to study speed. *Science*, *317*(5840), 905–906. https://doi.org/10.1126/science.1142143

Deldicque, D., Rouzaud, J. N., & Velde, B. (2016). A Raman-HRTEM study of the carbonization of wood: A new Raman-based paleothermometer dedicated to archaeometry. *Carbon*, *102*, 319–329. https://doi.org/10.1016/j.carbon.2016.02.042

Di Toro, G., Han, R., Hirose, T., De Paola, N., Nielsen, S., Mizoguchi, K., et al. (2011). Fault lubrication during earthquakes. *Nature*, *471*(7339), 494–498. https://doi.org/10.1038/nature09838

Di Toro, G., Hirose, T., Nielsen, S., Pennacchioni, G., & Shimamoto, T. (2006). Natural and experimental evidence of melt lubrication of faults during earthquakes. *Science*, *311*(5761), 647–649. https://doi.org/10.1126/science.1121012

Ferrand, T. P., Labrousse, L., Eloy, G., Fabbri, O., Hilairet, N., & Schubnel, A. (2018). Energy balance from a mantle pseudotachylyte, Balmuccia, Italy. *Journal of Geophysical Research: Solid Earth*, *123*, 3943–3967. https://doi.org/10.1002/2017JB014795

Goldsby, D. L., & Tullis, T. E. (2011). Flash heating leads to low frictional strength of crustal rocks at earthquake slip rates. *Science*, *334*(6053), 216–218. https://doi.org/10.1126/science.1207902

Green, H. W., Shi, F., Bozhilov, K., Xia, G., & Reches, Z. (2015). Phase transformation and nanometric flow cause extreme weakening during fault slip. *Nature Geoscience*, *8*(6), 484–489. https://doi.org/10.1038/ngeo2436

Griffith, A. A. (1920). The phenomena of flow and rupture in solids. *Philosophical Transactions of the Royal Society of London Series*, *221*(582-593), 163–198. https://doi.org/10.1098/rsta.1921.0006

Hayward, K. S., Cox, S. F., Fitz Gerald, J. D., Slagmolen, B. J. J., Shaddock, D. A., Forsyth, P. W. F., et al. (2016). Mechanical amorphization, flash heating, and frictional melting: Dramatic changes to fault surfaces during the first millisecond of earthquake slip. *Geology*, *44*(12), 1043–1046. https://doi.org/10.1130/G38242.1

Hirose, T., & Shimamoto, T. (2005). Growth of molten zone as a mechanism of slip weakening of simulated faults in gabbro during frictional melting. *Journal of Geophysical Research*, *110*, B05202. https://doi.org/10.1029/2004JB003207

Ide, S. (2002). Estimation of radiated energy of finite-source earthquake models. *Bulletin of the Seismological Society of America*, *92*(8), 2994–3005. https://doi.org/10.1785/0120020028

Ide, S., Beroza, G. C., Shelly, D. R., & Uchide, T. (2007). A scaling law for slow earthquakes. *Nature*, *447*(7140), 76–79. https://doi.org/10.1038/nature05780

Ito, K., Ujiie, K., & Kagi, H. (2017). Detection of increased heating and estimation of coseismic shear stress from Raman spectra of carbonaceous material in pseudotachylytes. *Geophysical Research Letters*, *44*, 1749–1757. https://doi.org/10.1002/2016GL072457

Kanamori, H., & Brodsky, E. E. (2004). The physics of earthquakes. *Reports on Progress in Physics*, *67*(8), 1429–1496. https://doi.org/10.1088/0034-4885/67/8/R03

Kanamori, H., & Rivera, L. (2006). *Energy partitioning during an earthquake. In Earthquakes: Radiated Energy and the Physics of Faulting*, *AGU Monograph Series* (Vol. 170, pp. 3–13). Washington, DC. https://doi.org/10.1029/170GM03

Kaneki, S., Ichiba, T., & Hirono, T. (2018). Mechanochemical effect on maturation of carbonaceous material: Implications for thermal maturity as a proxy for temperature in estimation of coseismic slip parameters. *Geophysical Research Letters*, *45*, 2248–2256. https://doi.org/10.1002/2017GL076791

Kirilova, M., Toy, V., Rooney, J. S., Giorgetti, C., Gordon, K. C., Collettini, C., & Takeshita, T. (2018). Structural disorder of graphite and implications for graphite thermometry. *Journal of Geophysical Research: Solid Earth*, *9*, 223–231. https://doi.org/10.5194/se-9-223-2018

Lay, T., Kanamori, H., Ammon, C. J., Koper, K. D., Hutko, A. R., Ye, L., et al. (2012). Depth-varying rupture properties of subduction zone megathrust faults. *Journal of Geophysical Research*, *117*, B04311. https://doi.org/10.1029/2011JB009133

Lockner, D. A., Kilgore, B. D., Beeler, N. M., & Moore, D. E. (2017). The transition from frictional sliding to shear melting in laboratory stick-slip experiments. In M. Y. Thomas, T. M. Mitchell, & H. S. Bhat (Eds.), *Fault zone dynamic processes: Evolution of fault properties during seismic rupture, Geophysical Monograph Series* (Chap. 6, pp. 105–130). Hoboken, NJ: American Geophysical Union.

Ma, K. F., Tanaka, H., Song, S. R., Wang, C. Y., Hung, J. H., Tsai, Y. B., Mori, J., et al. (2006). Slip zone and energetics of a large earthquake from the Taiwan Chelungpu-fault drilling project. *Nature*, *444*(7118), 473–476. https://doi.org/10.1038/nature05253

Madariaga, R. (1976). Dynamics of an expanding circular fault. *Bulletin of the Seismological Society of America*, *66*(3), 639–666.

Madariaga, R., Olsen, K., & Archuleta, R. (1998). Modeling dynamic rupture in a 3D earthquake fault model. *Bulletin of the Seismological Society of America*, *88*(5), 1182–1197.

Mitchell, T. M., Toy, V., Di Toro, G., Renner, J., & Sibson, R. H. (2016). Fault welding by pseudotachylyte formation. *Geology*, *44*(12), 1059–1062. https://doi.org/10.1130/G38373.1

Nielsen, S., Di Toro, G., Hirose, T., & Shimamoto, T. (2008). Frictional melt and seismic slip. *Journal of Geophysical Research*, *113*, B01308. https://doi.org/10.1029/2007JB005122

Nielsen, S., Spagnuolo, E., Violay, M., Smith, S., di Toro, G., & Bistacchi, A. (2016). G: Fracture energy, friction and dissipation in earthquakes. *Journal of Seismology*, *20*(4), 1187–1205. https://doi.org/10.1007/s10950-016-9560-1

Noda, H., Lapusta, N., & Kanamori, H. (2013). Comparison of average stress drop measures for ruptures with heterogeneous stress change and implications for earthquake physics. *Geophysical Journal International*, *193*(3), 1691–1712. https://doi.org/10.1093/gji/ggt074

Ohnaka, M. (2003). A constitutive scaling law and a unified comprehension for frictional slip failure, shear fracture of intact rock, and earthquake rupture. *Journal of Geophysical Research*, *108*(B2), 2080. https://doi.org/10.1029/2000JB000123

Passelègue, F. X., Schubnel, A., Nielsen, S., Bhat, H. S., Deldicque, D., & Madariaga, R. (2016). Dynamic rupture processes inferred from laboratory microearthquakes. *Journal of Geophysical Research: Solid Earth*, *121*, 4343–4365. https://doi.org/10.1002/2015JB012694

Passelègue, F. X., Schubnel, A., Nielsen, S., Bhat, H. S., & Madariaga, R. (2013). From sub-Rayleigh to supershear ruptures during stick-slip experiments on crustal rocks. *Science*, *340*(6137), 1208–1211. https://doi.org/10.1126/science.1235637

Renard, F., Beauprêtre, S., Voisin, C., Zigone, D., Candela, T., Dysthe, D. K., & Gratier, J. P. (2012). Strength evolution of a reactive frictional interface is controlled by the dynamics of contacts and chemical effects. *Earth and Planetary Science Letters*, *341-344*, 20–34. https://doi.org/10.1016/j.epsl.2012.04.048

Rice, J. R. (2006). Heating and weakening of faults during earthquake slip. *Journal of Geophysical Research*, *111*, B09314. https://doi.org/10.1029/2005JB004006

Savage, H. M., Polissar, P. J., Sheppard, R., Rowe, C. D., & Brodsky, E. E. (2014). Biomarkers heat up during earthquakes: New evidence of seismic slip in the rock record. *Geology*, *42*(2), 99–102. https://doi.org/10.1130/G34901.1

Scholz, C. H. (1986). *Preface: A short geophysical history of westerly granite*, *Geophysical Monograph Series* (Vol. 37). Washington, DC: American Geophysical Union. https://doi.org/10.1029/GM037p00ix

Schubnel, A., Brunet, F., Hilairet, N., Gasc, J., Wang, Y., & Green, H. W. (2013). Deep-focus earthquake analogs recorded at high pressure and temperature in the laboratory. *Science*, *341*(6152), 1377–1380. https://doi.org/10.1126/science.1240206

Schubnel, A., Fortin, J., Burlini, L., & Gueguen, Y. (2005). Damage and recovery of calcite rocks deformed in the cataclastic regime. *Geological Society, London, Special Publications*, *245*(1), 203–221. https://doi.org/10.1144/GSL.SP.2005.245.01.10

Tinti, E., Spudich, P., & Cocco, M. (2005). Earthquake fracture energy inferred from kinematic rupture models on extended faults. *Journal of Geophysical Research*, *110*, B12303. https://doi.org/10.1029/2005JB003644

Ujiie, K., Yamaguchi, H., Sakaguchi, A., & Toh, S. (2007). Pseudotachylytes in an ancient accretionary complex and implications for melt lubrication during subduction zone earthquakes. *Journal of Structural Geology*, *29*(4), 599–613. https://doi.org/10.1016/j.jsg.2006.10.012

Venkataraman, A., & Kanamori, H. (2004). Observational constraints on the fracture energy of subduction zone earthquakes. *Journal of Geophysical Research*, *109*, B05302. https://doi.org/10.1029/2003JB002549

Verberne, B. A., de Bresser, J. H. P., Niemeijer, A. R., Spiers, C. J., de Winter, D. A. M., & Plümper, O. (2013). Nanocrystalline slip zones in calcite fault gouge show intense crystallographic preferred orientation: Crystal plasticity at sub-seismic slip rates at 18–150°C. *Geology*, *41*(8), 863–866. https://doi.org/10.1130/G34279.1

Wald, D. J., & Heaton, T. H. (1994). Spatial and temporal distribution of slip for the 1992 Landers, California, earthquake. *Bulletin of the Seismological Society of America*, *84*(3), 668–691.

Wald, D. J., Heaton, T. H., & Hudnut, K. W. (1996). The slip history of the 1994 Northridge, California, earthquake determined from strong-motion, teleseismic, GPS, and leveling data. *Bulletin of the Seismological Society of America*, *86*(1B), S49–S70.

Wibberley, C. A., & Shimamoto, T. (2005). Earthquake slip weakening and asperities explained by thermal pressurization. *Nature*, *436*(7051), 689–692. https://doi.org/10.1038/nature03901

Wong, T.-F. (1982). Shear fracture energy of westerly granite from post-failure behavior. *Journal of Geophysical Research*, *87*(B2), 990–1000. https://doi.org/10.1029/JB087iB02p00990